HAL open science

Changes in Gut Microbiota by Chronic Stress Impair the Efficacy of Fluoxetine

Eleni Siopi, Grégoire Chevalier, Lida Katsimpardi, Soham Saha, Mathilde Bigot, Carine Moigneu, Gérard Eberl, Pierre-Marie Lledo

To cite this version:

Eleni Siopi, Grégoire Chevalier, Lida Katsimpardi, Soham Saha, Mathilde Bigot, et al.. Changes in Gut Microbiota by Chronic Stress Impair the Efficacy of Fluoxetine. Cell Reports, 2020, 30 (11), pp.3682 - 3690.e6. 10.1016/j.celrep.2020.02.099 . pasteur-03257987

HAL Id: pasteur-03257987

https://pasteur.hal.science/pasteur-03257987v1

Submitted on 11 Jun 2021

HAL is a multi-disciplinary open access archive for the deposit and dissemination of scientific research documents, whether they are published or not. The documents may come from teaching and research institutions in France or abroad, or from public or private research centers.

L'archive ouverte pluridisciplinaire **HAL**, est destinée au dépôt et à la diffusion de documents scientifiques de niveau recherche, publiés ou non, émanant des établissements d'enseignement et de recherche français ou étrangers, des laboratoires publics ou privés.

Distributed under a Creative Commons Attribution - NonCommercial - NoDerivatives 4.0 International License

Report

Cell Reports

Changes in Gut Microbiota by Chronic Stress Impair the Efficacy of Fluoxetine

Graphical Abstract

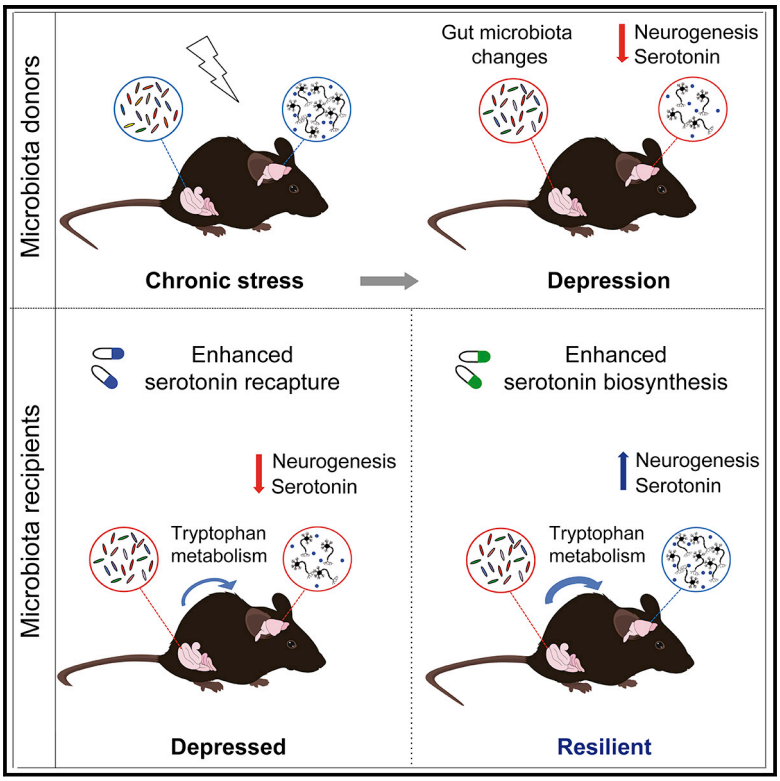

Highlights

- UCMS induces changes in the GM
- GM from UCMS mice induces depression and decreases HpC neurogenesis in healthy mice
- GM from UCMS mice impairs the serotonergic pathway of Trp metabolism
- Promoting 5-HT biosynthesis alleviates the symptoms of GM-induced depression

Authors

Eleni Siopi, Grégoire Chevalier, Lida Katsimpardi, ..., Carine Moigneu, Gérard Eberl, Pierre-Marie Lledo

Correspondence

eleni.siopi@inserm.fr (E.S.), pmlledo@pasteur.fr (P.-M.L.)

In Brief

Siopi et al. demonstrate that perturbations in the gut microbiota by chronic stress induce resistance to serotonergic antidepressants via impairments in serotonin biosynthesis and bioavailability. Supplementation with the immediate serotonin precursor 5-hydroxytrytophan restores serotonin levels and neurogenesis in the hippocampus and confers resilience.

Siopi et al., 2020, Cell Reports *30*, 3682–3690
March 17, 2020 © 2020 The Authors.
https://doi.org/10.1016/j.celrep.2020.02.099

OPEN ACCESS
CellPress

Cell Reports
Report

Changes in Gut Microbiota by Chronic Stress Impair the Efficacy of Fluoxetine

Eleni Siopi,[1,2,6,*] Grégoire Chevalier,[3,4,5] Lida Katsimpardi,[1,2,5] Soham Saha,[1,2,5] Mathilde Bigot,[1,2] Carine Moigneu,[1,2] Gérard Eberl,[3,4] and Pierre-Marie Lledo[1,2,*]
[1]Institut Pasteur, Perception and Memory Unit, 75015 Paris, France
[2]Centre National de la Recherche Scientifique (CNRS), Unité Mixte de Recherche 3571, 75015 Paris, France
[3]Institut Pasteur, Microenvironment and Immunity Unit, 75724 Paris, France
[4]Institut National de la Santé et de la Recherche Médicale (INSERM) U1224, 75724 Paris, France
[5]These authors contributed equally
[6]Lead Contact
*Correspondence: eleni.siopi@inserm.fr (E.S.), pmlledo@pasteur.fr (P.-M.L.)
https://doi.org/10.1016/j.celrep.2020.02.099

SUMMARY

Major depressive disorders (MDDs) constitute a leading cause of disability worldwide and current pharmacological treatments are partially effective. The gut microbiota (GM) has recently emerged as a target of therapeutic interest for MDDs. In this study, we transfer GM from mice that sustained unpredictable chronic mild stress (UCMS) to healthy recipient mice. The fecal transfer induces despair-like behavior, decreases neurogenesis in the hippocampus (HpC), and impairs the antidepressant and neurogenic effects of a standard selective serotonin (5-HT) reuptake inhibitor, fluoxetine (FLX). These effects are paralleled by deficits in 5-HT bioavailability, biosynthesis, and reuptake in the HpC. Treatment with 5-hydroxytryptophan restores the levels of 5-HT and its precursors in the HpC, improves HpC neurogenesis, and alleviates despair-like symptoms. Our results reveal that stress-induced changes in GM are involved in the pathogenesis of depressive disorders and minimize FLX efficacy via alterations in the serotonergic pathway of Trp metabolism.

INTRODUCTION

Major depressive disorders (MDDs) constitute a leading cause of disability worldwide (Kassebaum and GBD 2015 DALYs and HALE Collaborators, 2016). Although current antidepressants (ADs), such as selective serotonin (5-HT) reuptake inhibitors (SSRIs), help many patients recover, high rates of partial or no response leave many patients inadequately treated, leading to debates about their efficacy (Ioannidis, 2008). The identification of new targets of therapeutic interest or factors that could ameliorate AD drug efficacy is therefore of crucial importance for health care.

The most significant risk determinant for MDDs is chronic stress (Nestler et al., 2002). One factor that is highly sensitive to chronic stress and that is impacted in MDDs is the gut microbiota (GM) (Naseribafrouei et al., 2014; De Palma et al., 2015; Jiang et al., 2015; Zheng et al., 2016; Marin et al., 2017). Various studies have shown that the GM is strongly implicated in whole host metabolism (Velagapudi et al., 2010; Desbonnet et al., 2015), namely, tryptophan (Trp) availability (Clarke et al., 2013; O'Mahony et al., 2015). Importantly, the efficacy of SSRI treatments depends on the availability of synaptic 5-HT and, therefore, on Trp catabolism (Ressler and Nemeroff, 2000). However, no study so far has addressed the question of whether GM can affect SSRI drug efficacy.

Here, we hypothesize that stress-induced GM perturbations could be responsible for metabolic changes impacting affective behavior and serotonergic drug responsiveness. To test this hypothesis, we used a model of chronic stress-induced depression to study the effect of GM on the antidepressant and neurogenic effects of a standard SSRI, fluoxetine (FLX).

RESULTS

GM Transfer from UCMS Mice Promotes Depression and Decreases HpC Neurogenesis in Host Mice

To determine whether the transfer of GM from stressed mice affects mood states and adult neurogenesis in healthy recipient mice, we used the unpredictable chronic mild stress (UCMS) model. Mice treated with antibiotics (abx) were inoculated with GM harvested from UCMS mice (Figures 1A–1C). UCMS induced despair-like behavior, as depicted by immobility in the tail suspension test (TST; Figure 1G) and forced swim test (FST; Figure 1I). Both tests measure the amount of time an animal struggles to escape an uncomfortable situation, a behavior typically affected in models of depression and corrected by AD treatment. We next looked at adult neurogenesis in the dentate gyrus (DG) of the hippocampus (HpC), which is consistently impaired in models of depression (Nestler et al., 2002). We found that the number of cells expressing DCX, a marker of transient proliferating mitotic neuronal progenitor cells, was significantly decreased (Figures 1D and 1F). Recipient mice adopted a similar phenotype, characterized by despair-like behavior (Figures 1H and 1J) and a decrease in the number of DCX^+ cells in the DG (Figures 1E and 1F). Abx treatment did not affect behavior and HpC neurogenesis (Figures S3O and S3P). These results reveal that healthy mice develop despair-like behaviors and deficits in HpC neurogenesis after inoculation with GM from UCMS mice.

 © 2020 The Authors.
This is an open access article under the CC BY-NC-ND license (http://creativecommons.org/licenses/by-nc-nd/4.0/).

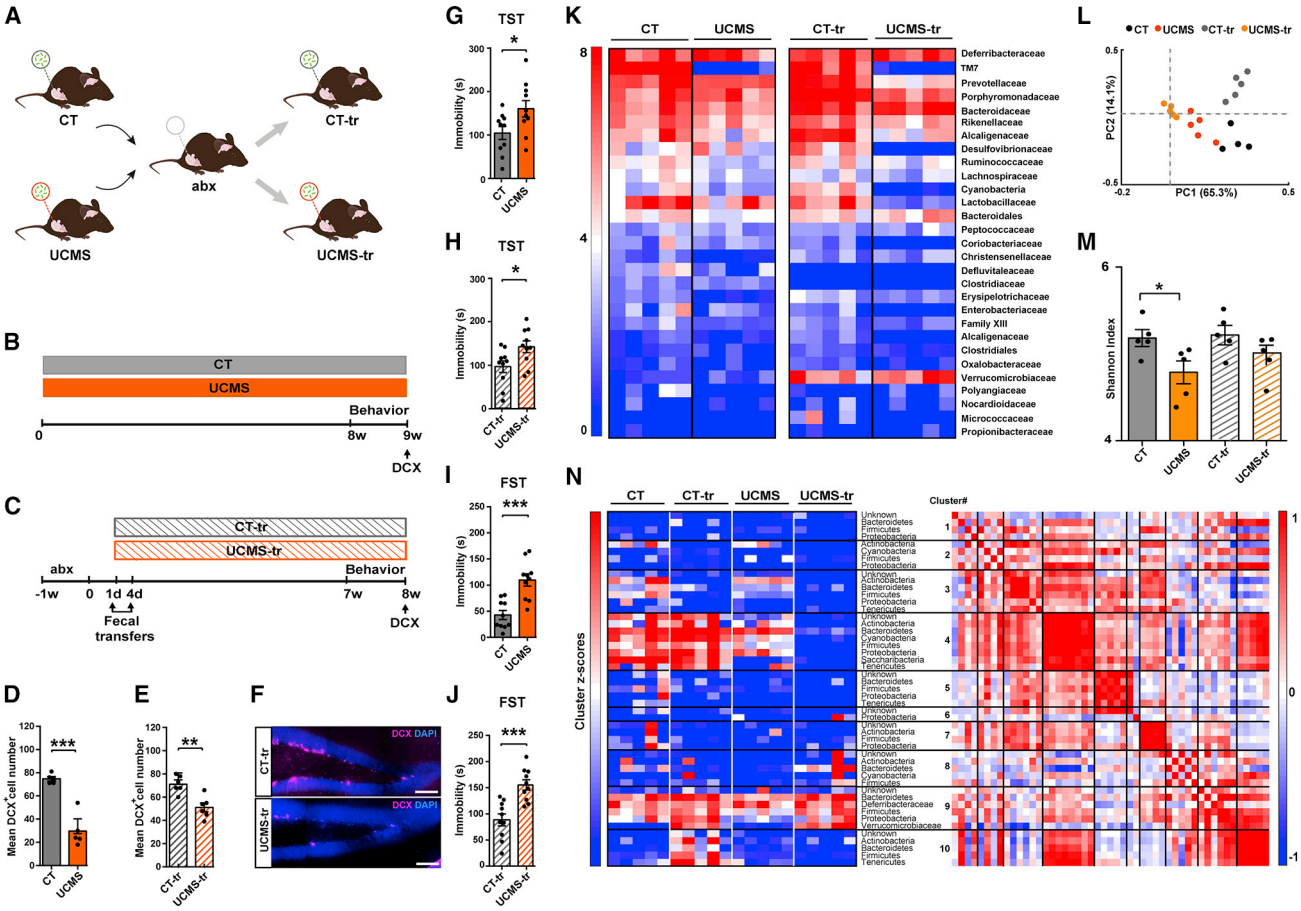

Figure 1. Transfer of GM from UCMS Mice Induces Despair-like States and Decreases Neurogenesis in Healthy Recipient Mice

(A) Schematic illustration of the fecal transplantation paradigm and the groups used in the study.

(B and C) Experimental designs used for assessing GM changes and behavior in microbiota donor, CT and UCMS (B), and recipient, CT-tr and UCMS-tr (C), mice.

(D and E) The total number of DCX^+ neurons was decreased in both UCMS ($p = 0.001$) (D) and UCMS-tr ($p = 0.002$) (E) mice.

(F) Representative images of DCX^+ neurons in a section of DG from CT-tr and UCMS-tr mice. Scale bars: 100 μm.

(G and H) Immobility in the TST was increased in UCMS mice ($p = 0.03$) (G) and in mice that received UCMS microbiota ($p = 0.03$) (H).

(I and J) Immobility in the FST was significantly increased in both UCMS ($p = 0.0002$) (I) and UCMS-tr ($p = 0.0003$) (J) mice.

(K) Heatmap showing 16S rRNA expression patterns in different experimental conditions. Bacterial families are shown in the right, and heatmap scale is 0–8.

(L) PCoA of 16S rRNA expression data showing group differences in principal-coordinate axes (PC1: 65.3% and PC2: 14.1%).

(M) Bar plots showing a reduction of the Shannon Index with UCMS compared with CT ($p = 0.05$) and a trend of reduction with UCMS-tr compared with CT-tr.

(N) Isolation and annotation of the bacterial phyla and families identified by clustering methods, followed by representation of the clusters as a heatmap. Scale of cluster Z scores is 0–1. (Right) Autocorrelation showing the identical expression of variability of each cluster across the groups. Autocorrelation matrix scale: −1 to 1. Data are shown as mean ± SEM.

abx, antibiotics; DCX, doublecortin; DG, dentate gyrus; FST, forced swim test; TST, tail suspension test. See also Figures S1 and S3.

Stress-Induced Changes in GM Are Transferrable to Host Mice

In light of these results, we examined the GM profile by 16S rRNA sequencing. We first confirmed that abx significantly decreased microbial diversity as expected (Figures S3A–S3D). Taxonomic analysis of bacterial families revealed several UCMS-related changes in GM composition, most of which were transferred to UCMS-tr mice (Figures 2K–2N; Figure S1). Principal-coordinate analysis (PCoA) showed that the different groups clustered differently (Figure 1L). It is to be noted that the relative dispersion between the points corresponding to UCMS and UCMS-tr was not significant (Bray-Curtis index; data not shown). These changes were also detectable in phylum level, namely, in Firmicutes, Tenericutes, and candidate division TM7 (Figures S1B, S1G, and S1H). Moreover, microbial diversity, as depicted by the Shannon Index, was decreased in UCMS and UCMS-tr mice (Figure 1M). Furthermore, we categorized the most variable bacterial families and phyla in between groups using a correlation network methodology (Figure 1N; Figures S1N and S1O). This type of cluster analysis further helped us to account for the effects of abx on different groups of bacteria (Figures S3B and S3C).

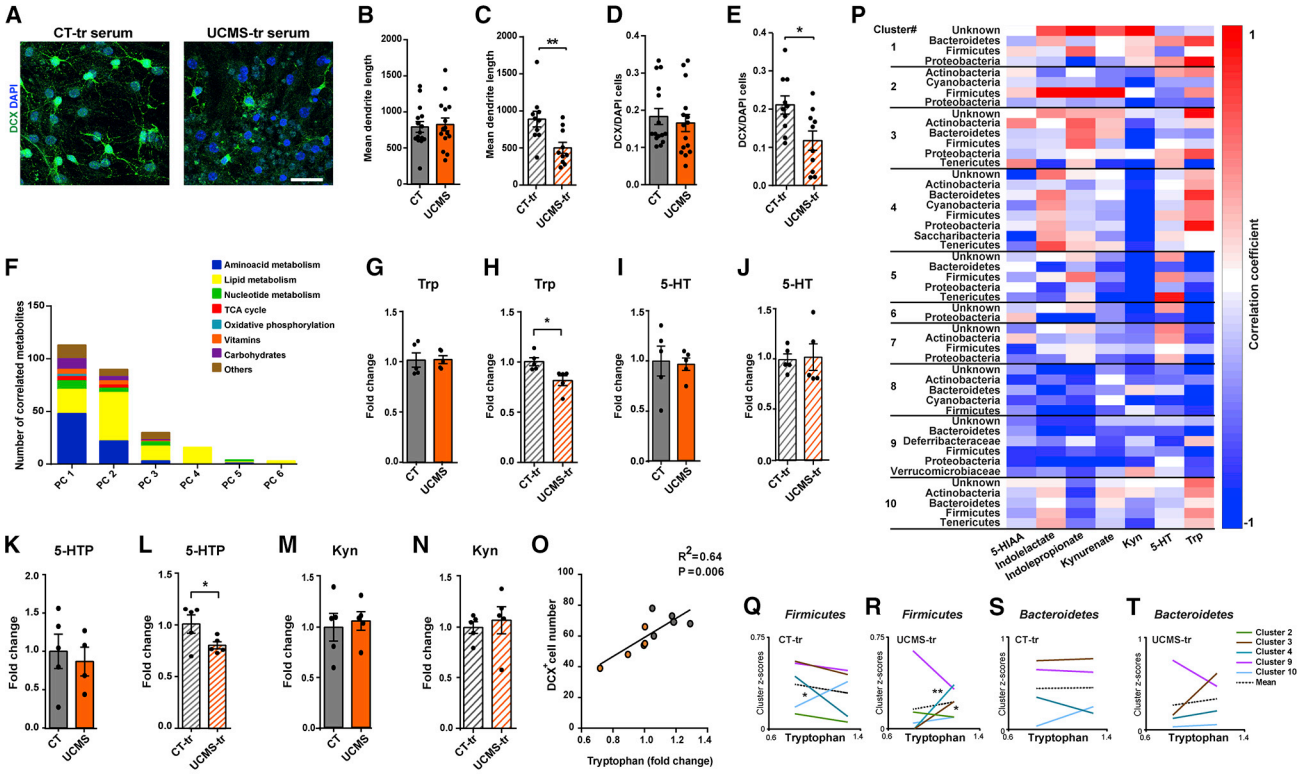

Figure 2. Inoculation with UCMS Microbiota Impairs Trp Metabolism

(A) Representative images of DCX$^+$ neurons in neurosphere cultures treated with serum extracted from either CT-tr or UCMS-tr recipient mice. Scale bar: 30 μm.

(B–E) Serum from UCMS-tr mice significantly decreased the number of DCX$^+$ cells ($p = 0.02$) and mean dendrite length ($p = 0.003$) in neurosphere cultures.

(F) PCA of serum metabolite levels revealed significant changes in amino acid levels.

(G–N) Bar plots depicting serum levels of Trp, 5-HT, 5-HTP, and Kyn in GM donor (CT, UCMS) and recipient (CT-tr, UCMS-tr) mice. UCMS-tr mice had significantly lower levels of Trp ($p = 0.03$) and 5-HTP ($p = 0.05$).

(O) Scatterplot demonstrating the positive correlation between the number of DCX$^+$ neurons and Trp levels in recipient mice ($R^2 = 0.64$, $p = 0.006$).

(P) Correlation heatmap of the clusters of bacteria identified by Weighted Gene Correlation Network Analysis (WGCNA) (Figures S2N and S2O) against the major serum Trp metabolites. Heatmap scale is 0–1.

(Q–T) Individual trends of Trp variation with clusters corresponding to Firmicutes and Bacteroidetes. Data are shown as mean ± SEM.

See also Figures S2–S4.

Serum from UCMS-tr Mice Decreases Neural Stem Cell Differentiation

Given the key role of GM in metabolism, we asked whether GM transfer could impact HpC neurogenesis by changing the levels of serum metabolites. To answer this question, we isolated serum from donor and recipient mice, and applied the different sera on an *in vitro* heterogeneous population of neural stem and progenitor cells. We measured the total number of DCX$^+$ cells, as well as mean dendrite length, as a proxy of neurite outgrowth. Our results showed that sera derived from UCMS-tr mice significantly decreased dendrite length (Figures 2A and 2C) and DCX$^+$ cell number (Figures 2A and 2E), suggesting changes in serum composition that affect neural stem cell differentiation. Sera from UCMS mice had no impact on neurospheres (Figures 2A, 2B, and 2D), suggesting that other pathways are preferentially involved in UCMS-induced neurogenesis deficits. Treatment of neural stem cells with sera harvested from abx-treated mice did not affect neuronal differentiation (Figures S3J and S3K).

Inoculation with UCMS-Microbiota Impairs Trp Metabolism

We then performed untargeted metabolomic analysis to identify the molecular signature in the serum that could explain these results. Principal-component analysis (PCA) revealed that amino acid metabolism was the most affected pathway (Figure 2F; Figure S2). UCMS-tr mice had significantly lower levels of 5-HT's precursor, Trp (Figure 2H), and its immediate precursor, 5-hydroxytryptophan (5-HTP) (Figure 2L), although 5-HT and kynurenine (Kyn) levels were not changed (Figures 2J and 2N). Trp and its metabolites were unchanged in UCMS mice (Figures 2G, 2I, 2K, and 2M). We also observed that the level of 5-hydroxyindoleacetic acid (5-HIAA), a product of 5-HT catabolism, was increased in UCMS-tr mice (Figures S4A, S4B, and S4K), whereas metabolites belonging to the Kyn or indole derivative pathway did not seem significantly affected by either UCMS or the transfer of UCMS microbiota (Figures S4C–S4G). Interestingly, we found a significant correlation between Trp levels and the number of DCX$^+$ neurons in the DG (Figure 2O). Concerning

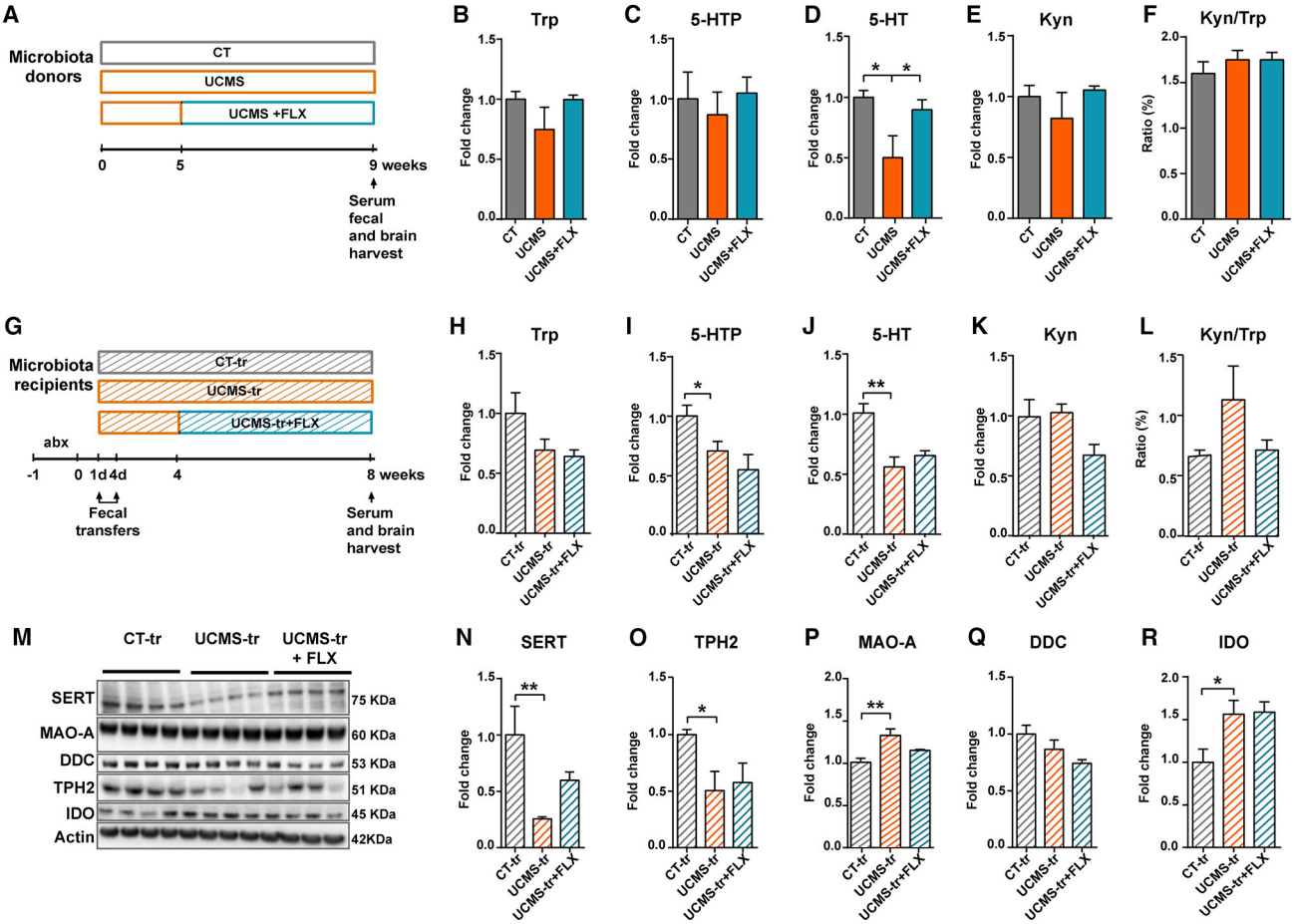

Figure 3. Selective 5-HT Reuptake Inhibitor FLX Does Not Restore 5-HT Availability in the HpC of UCMS-tr Mice

(A) Experimental design used for assessing the effect of FLX in mice that sustained UCMS.

(B–F) Bar plots depicting the levels of (B) Trp, (C) 5-HTP, (D) 5-HT, (E) Kyn, and the (F) Kyn/Try ratio in the HpC. 5-HT levels were significantly decreased in UCMS mice ($p = 0.015$) and restored by FLX ($p = 0.04$).

(G) Experimental design used for assessing the effect of FLX in UCMS-tr mice.

(H–L) Bar plots showing levels of (H) Trp, (I) 5-HTP, (J) 5-HT, (K) Kyn, and the (L) Kyn/Try ratio in the HpC. UCMS-tr mice had significantly lower levels of 5-HTP ($p = 0.03$) and 5-HT ($p = 0.001$) that were not restored by FLX.

(M) Representative western blots of SERT, MAO-A, DDC, TPH2, and IDO in the HpC.

(N–R) Bar plots depicting HpC levels of (N) SERT, (O) TPH2, (P) MAO-A, (Q) DDC, and (R) IDO relative to CT-tr. UCMS-tr mice had significantly lower levels of SERT ($p = 0.01$) and TPH2 ($p = 0.05$), and higher levels of MAO-A ($p = 0.005$) and IDO ($p = 0.04$). Data are shown as mean ± SEM.

the gut, UCMS-tr mice had lower levels of Trp and 5-HT, and a decrease in mean Kyn levels (Figures S4M–S4O). Finally, we found that abx did not change 5-HT and Kyn serum levels, but affected 5-HT levels in the gut (Figures S3E–S3I).

Changes in Serum Trp Levels Correlate with GM Changes

Using a correlation matrix, we found correlations between identified clusters of GM and Trp metabolites, namely Trp (Figure 2P). We isolated the most prominent bacteria phyla in each cluster, the Firmicutes and Bacteroidetes, and correlated them to the Trp expression profile. We found that changes in Trp levels with respect to bacterial variations in control (CT)/CT-tr and UCMS/UCMS-tr were positive in the case of clusters 4 and 10 (Figure 2P). By applying the same method, we found that abx eradicate the specific microbial clusters that were identified as highly correlated to Trp, i.e., clusters 4 and 10 (Figures S3B and S3C).

GM from UCMS Mice Decrease 5-HT Biosynthesis in the HpC

Taking into account that serum Trp levels predict brain 5-HT synthesis (Fernstrom et al., 2013), potentially impacting response to serotonergic treatment, we checked brain levels of Trp, 5-HTP, and 5-HT. Based on our results showing deficits in HpC neurogenesis, we chose to focus on the HpC for our analysis. We found that UCMS did not affect the levels of Trp and 5-HTP (Figures 3B and 3C), but decreased 5-HT levels (Figure 3D). We then checked whether this decrease in 5-HT was due to a preferential catabolism of Trp toward the Kyn pathway

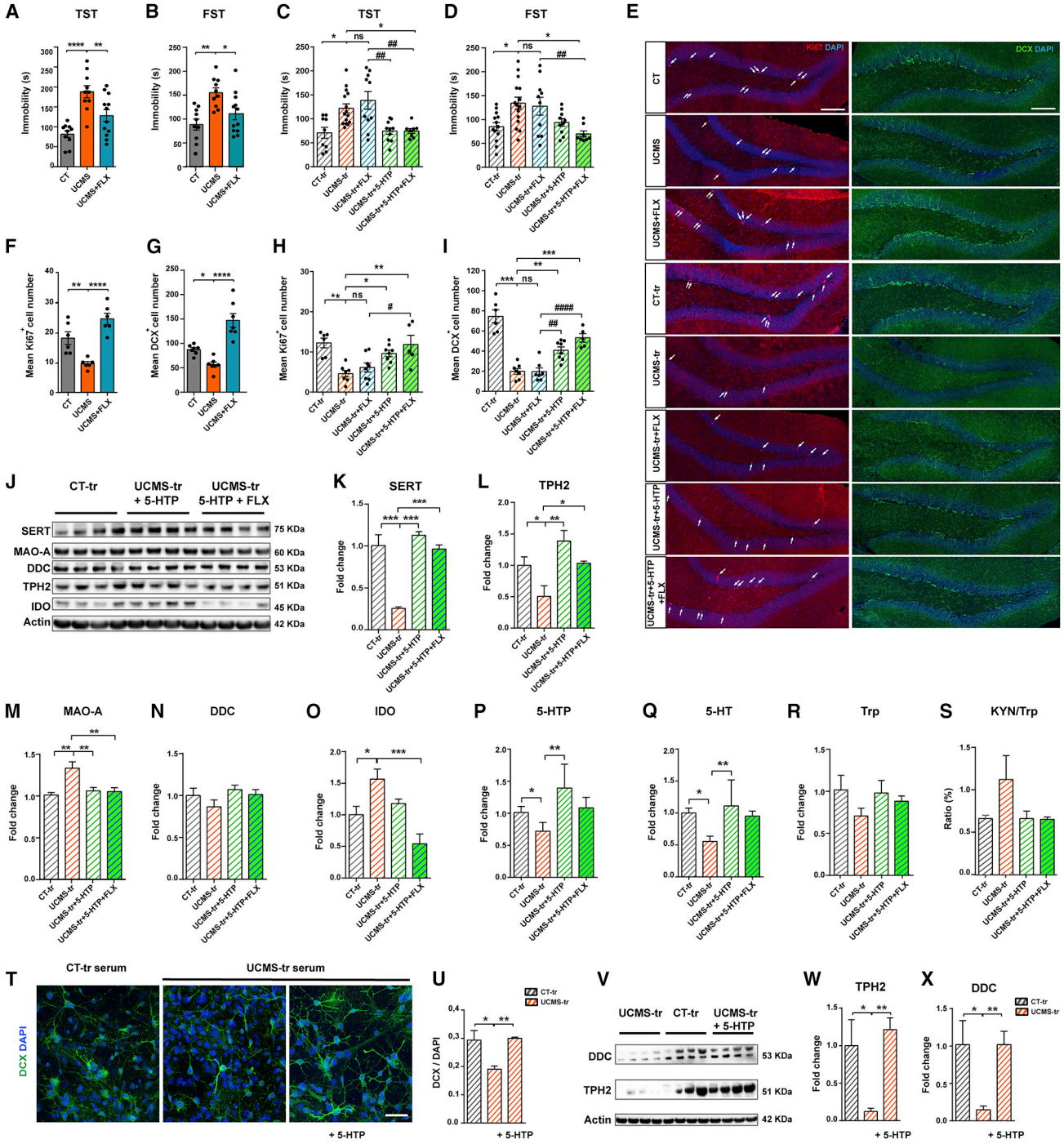

Figure 4. Restoration of 5-HT Biosynthesis Alleviates Depressive Symptoms and Restores Neurogenesis in UCMS-tr Mice

(A and B) Graphs depicting immobility in the (A) TST and (B) FST. FLX restored immobility in the TST ($p = 0.009$) and FST ($p = 0.02$).

(C and D) FLX did not restore despair-like behavior, but 5-HTP decreased immobility in both the (C) TST ($p = 0.02$ versus UCMS-tr; $p = 0.002$ versus UCMS-tr+FLX) and (D) FST ($p = 0.03$ versus UCMS-tr; $p = 0.006$ versus UCMS-tr+FLX).

(E) Representative images of $Ki67^+$ and DCX^+ cells in the DG. White arrows indicate $Ki67^+$ cells. Scale bars: 100 μm.

(F and G) Bar plots of the number of (F) $Ki67^+$ and (G) DCX^+ cells in the DG. UCMS decreased both $Ki67^+$ and DCX^+ cell numbers, and FLX attenuated this decrease ($p < 0.0001$).

(H and I) 5-HTP restored the number of $Ki67^+$ ($p = 0.02$) cells and DCX^+ neurons ($p = 0.01$) in UCMS-tr mice. Data are shown as mean ± SEM.

(J) Representative western blots of SERT, MAO-A, DDC, TPH2, and IDO in the HpC.

(legend continued on next page)

and found that Kyn levels were unchanged (Figures 3E and 3F). Interestingly, we observed that UCMS-tr mice had significantly lower levels of both 5-HTP and 5-HT (Figures 3I and 3J). Kyn levels were not significantly higher in UCMS-tr mice, although the mean Kyn/Trp ratio was increased (Figures 3K and 3L). Next, we investigated the expression levels of the enzymes participating in these metabolic pathways. We found that the levels of the 5-HT transporter (SERT), which mediates 5-HT reuptake from the synaptic cleft, and Trp hydroxylase 2 (TPH2), the enzyme catalyzing the conversion of Trp to 5-HTP, were significantly decreased in UCMS-tr mice, whereas the levels of the 5-HT degradation enzyme, monoamine oxidase inhibitor A (MAO-A), were increased (Figures 3M–3P). Dopamine decarboxylase (DDC) levels were not changed, whereas the levels of indoleamine oxygenase (IDO), the enzyme that catalyzes Trp conversion to Kyn, were increased (Figures 3M, 3Q, and 3R).

FLX Does Not Restore Brain 5-HT Levels in UCMS-tr Mice

In view of these results, we asked whether these changes in 5-HT bioavailability could impact SSRI efficacy. To answer this question, we added cohorts of donor and recipient mice that were treated with FLX for 4 weeks (Figures 3A and 3G). We found that FLX successfully elevated 5-HT levels in the HpC of UCMS mice (Figure 3D), but not in UCMS-tr mice (Figure 3J). 5-HTP levels also remained unchanged by FLX (Figures 3C and 3I). We then studied the impact of FLX on the expression of enzymes and proteins related to 5-HT biosynthesis, degradation, and reuptake. We found that FLX did not restore the levels of SERT, which constitutes the target of SSRI action, in UCMS-tr mice (Figure 3N). Moreover, FLX did not change TPH2 or MAO-A levels (Figures 3O and 3P). Finally, we found that FLX did not restore IDO levels (Figure 3R).

GM from UCMS Mice Impede the Neurogenic and AD Effects of FLX

Next, we tested the behavioral and neurogenic effects of FLX on donor and recipient mice. As expected, FLX decreased immobility in UCMS donor mice both in the TST and the FST (Figures 4A and 4B). Moreover, FLX largely increased the number of Ki67$^+$ cells and DCX-expressing neuroblasts in UCMS mice (Figures 4E–4G). However, we found that FLX did not improve immobility (Figures 4C and 4D) and did not restore the levels of either Ki67$^+$ or DCX$^+$ cells in UCMS-tr mice (Figures 4E, 4H, and 4I).

5-HTP Restores HpC Neurogenesis and Alleviates Depression-like Symptoms

To investigate the implication of 5-HT biosynthesis in the lack of FLX efficacy, we tested whether treatment with the immediate 5-HT precursor, 5-HTP, alleviates depression-like symptoms in UCMS-tr mice. Both behavioral and neurogenesis readouts were analyzed. We found that 5-HTP completely rescued despair-like behavior in the TST and FST (Figures 4C and 4D), and restored the number of Ki67$^+$ and DCX$^+$ cells (Figures 4E, 4H, and 4I).

5-HTP Increases 5-HT Levels and Availability in the HpC

To further determine whether 5-HT biosynthesis is implicated in the restoration of the behavioral and neurogenesis deficits by 5-HTP, we measured the effect of 5-HTP on 5-HT, Try, and Kyn in the HpC, as well as on the levels of key enzymes implicated in these metabolic pathways. As expected, 5-HTP increased the levels of 5-HTP in the HpC (Figure 4P). This effect was associated with a significant increase in 5-HT (Figure 4Q) and a decrease in the mean levels of Kyn (Figure 4S). Interestingly, 5-HTP also significantly increased the HpC levels of SERT and TPH2 (Figures 4J–4L), whereas it decreased MAO-A (Figures 4J and 4M) and IDO levels (Figures 4J and 4O).

5-HTP Restores Neural Stem Cell Differentiation

In light of these results, we tested the effect of 5-HTP on neural stem cell differentiation. We applied sera from either CT-tr or UCMS-tr mice on neurosphere cultures and added 5-HTP in one subset of UCMS-tr-treated neurospheres. We confirmed that UCMS-tr sera impair neuronal differentiation, depicted by a decrease in DCX$^+$ cell number, and then observed that 5-HTP completely attenuated this impairment (Figures 4T and 4U). Moreover, we observed a significant decrease of TPH2 and DDC in the lysate of UCMS-tr-treated neurospheres and found that 5-HTP supplementation restored the levels of both enzymes (Figures 4V–4X).

DISCUSSION

We report here that inoculation with GM derived from chronically stressed mice induces despair-like behavior, decreases adult HpC neurogenesis, and impairs the serotonergic pathway of Trp metabolism in healthy recipient mice that become poorly responsive to SSRI treatment. Supplementation with 5-HTP, the immediate 5-HT precursor, alleviates despair symptoms and restores HpC neurogenesis. These effects are paralleled

(K–O) Bar plots depicting HpC levels of (K) SERT, (L) TPH2, (M) MAO-A, (N) DDC, and (O) IDO relative to CT-tr. 5-HTP restored HpC levels of SERT ($p < 0.001$), TPH2 ($p = 0.002$), and IDO (UCMS-tr+5-HTP+FLX versus UCMS-tr: $p = 0.0005$).
(P–R) Bar plots showing relative levels of (P) 5-HTP, (Q) 5-HT, and (R) Trp in the HpC. 5-HTP treatment increased 5-HTP ($p = 0.004$) and 5-HT ($p = 0.009$) levels in UCMS-tr mice.
(S) Bar plot displaying the Kyn/Trp ratio in the HpC.
(T) Representative images of DCX$^+$ neurons in neurosphere cultures treated with serum extracted from either CT-tr or UCMS-tr mice. A subset of NSC was treated with UCMS-tr serum supplemented with 5-HTP. Scale bar: 30 μm.
(U) 5-HTP restored the number of DCX$^+$ neurons in UCMS-tr-treated NSC.
(V) Images of western blots for DDC and TPH2 lysate from neurosphere cultures treated with either CT-tr or UCMS-tr serum, or with UCMS-tr serum supplemented with 5-HTP.
(W and X) UCMS-tr serum decreased (W) TPH2 ($p = 0.03$) and (X) DDC ($p = 0.03$) expression, and 5-HTP restored these effects (TPH2: $p = 0.01$; DDC: $p = 0.03$). Data are shown as mean ± SEM.
See also Figure S4.

by restoration of 5-HT biosynthesis. Understanding the role GM play in affective behaviors and response to treatments holds substantial potential for a successful therapeutic management of depressive disorders.

Mounting evidence shows that the GM act as a virtual endocrine organ, producing signals that trigger responses at both local and distant scales (Zhang and Davies, 2016). Given the key role of GM in host metabolism, perturbations of this complex ecosystem by chronic stress could impair the efficacy of AD treatments. The neurogenic hypothesis for MDDs points to impairments in adult HpC neurogenesis, and human studies also report reduced HpC volume in MDDs (Campbell et al., 2004; Sahay and Hen, 2007; Boldrini et al., 2013). Importantly, HpC neurogenesis is increased by ADs and confers resilience to chronic stress (Santarelli et al., 2003; Anacker et al., 2018). The contribution of 5-HT in adult HpC neurogenesis is widely accepted (Gould, 1999). Interestingly, intestinal dysbiosis has also been shown to produce deficits in HpC neurogenesis in mice (Möhle et al., 2016).

Our results support recent animal (De Palma et al., 2015; Marin et al., 2017) and human (Naseribafrouei et al., 2014; Jiang et al., 2015; Zheng et al., 2016) studies showing that GM composition is modified by chronic stress and depression. In our experimental conditions, although UCMS-tr mice adopted the bacterial profile of their donor counterparts, the transmitted perturbations were exacerbated. Our serum metabolomic analysis then revealed that UCMS-tr sera were characterized by a significant decrease in amino acids, whereas fewer changes were observed in UCMS sera. This discrepancy could be explained by the dramatic decrease of a specific cluster of GM, which we found to be positively correlated to Trp levels, specifically in UCMS-tr mice.

Our results suggest that the decrease in serum Trp and 5-HTP levels could be either GM and/or host dependent. The use of Trp by some gut bacterial strains for their own metabolism (Bouknight and Sadoff, 1975) could limit its availability for the host. Moreover, given that other essential amino acids were also decreased, the decrease in Trp could result from general dysbiosis-induced perturbations in nutrient absorption and bioavailability. Although our study did not identify a specific microbe responsible for the phenotype observed, our analysis revealed a correlation between the Firmicutes and Trp levels, suggesting that perturbations in microbes belonging to this phylum could be responsible for these changes.

Because brain 5-HT availability is strictly dependent on Trp released from the gut into the circulation (Agus et al., 2018), we assumed that lower serum Trp would reflect lower levels of brain 5-HT (Fernstrom et al., 2013). We found that although 5-HT was decreased in both UCMS and UCMS-tr hippocampi, its precursor 5-HTP was specifically decreased in the UCMS-tr condition, suggesting alterations in both 5-HT availability and biosynthesis. Interestingly, we found that TPH2 and SERT were drastically decreased, strongly indicating a deficit in 5-HTP production and 5-HT reuptake, and that MAO-A levels were increased, indicating an increase in 5-HT degradation. Collectively, these experiments reveal alterations in the biosynthesis, reuptake, and degradation of 5-HT.

Stimulation of adult HpC neurogenesis seems to be a prerequisite for AD efficacy, and it is achieved with different classes of pharmacological ADs (Perera et al., 2007; Surget et al., 2008, 2011; Schmuckermair et al., 2013). Our dysbiosis-induced depression model prevented a subset of the signature cellular and behavioral effects of FLX, a standard AD. FLX efficacy was accompanied by deficits in the serotonergic pathway of Trp metabolism. Our results are reminiscent of previous studies on *hydroxylase 2* knockin mice, which are resistant to FLX treatment due to congenital 5-HT deficiency unless treated with 5-HTP (Jacobsen et al., 2012; Sachs et al., 2013; Siesser et al., 2013). The key role of 5-HT deficiency was further confirmed when we showed that 5-HTP administration restored HpC neurogenesis and despair behavior, as well as the levels of SERT, TPH2, and MAO-A. These findings indicate that 5-HT biosynthesis is responsible, at least in part, for the resistance to FLX. To further confirm the role of 5-HT biosynthesis in neuronal differentiation, we showed that 5-HTP supplementation restored the number of DCX^+ neurons in UCMS-tr-treated neuronal stem cells, as well as the levels of TPH2 and DDC. Altogether, these results point to a role of Trp metabolism in neuronal differentiation and show that a decrease in 5-HT bioavailability, combined with deficits in 5-HT biosynthesis and reuptake, could explain the lack of efficacy of FLX, as well as the therapeutic gain of 5-HTP.

The fact that humans rely mostly on dietary Trp intake, whose metabolism is exclusively governed by microbiota (Agus et al., 2018), makes Trp an actionable actor for new therapeutic strategies in MDD. Exploiting microorganisms specifically involved in Trp catabolism should be considered as a potentially powerful tool to treat MDDs. Our study also suggests that plasma levels of Trp should be considered as a biomarker to orientate therapeutic choices in depressive disorders. Taken together, this study provides evidence that stress-induced dysbiosis can impair FLX efficacy via changes in Trp metabolism. Other non-mutually exclusive pathways could be also implicated, including vagal nerve innervation, neuroendocrine signaling, or neuroimmune regulation. Hence, as Agus et al. (2018) stated, combining metabolomics with metagenomics and metatranscriptomics approaches seems a promising strategy to identify the microbes and microbial genes involved in Trp metabolism. Once identified, novel therapies aiming at using genetically engineered bacteria to modulate Trp levels should be considered to further address the complex issue of treatment-resistant depression.

STAR★METHODS

Detailed methods are provided in the online version of this paper and include the following:

- KEY RESOURCES TABLE
- LEAD CONTACT AND MATERIALS AVAILABILITY
- EXPERIMENTAL MODEL AND SUBJECT DETAILS
  - Animals
  - Unpredictable chronic mild stress (UCMS) procedure
  - Treatments
  - Experimental sets
- METHOD DETAILS
  - Behavioral testing

- Tail suspension test
- Forced swim test
- Open field
- Elevated plus maze
- Light and dark box
- Animal sacrifice and tissue collection
- Neural stem cell cultures
- Western blots
- Sandwich ELISA immunoassays
- Immunofluorescence
- Confocal imaging and quantification
- Microbial DNA extraction and 16S sequencing
- 16S sequencing data analysis
- Serum extraction and metabolite analysis

- QUANTIFICATION AND STATISTICAL ANALYSIS
- DATA AND CODE AVAILABILITY

SUPPLEMENTAL INFORMATION

Supplemental Information can be found online at https://doi.org/10.1016/j.celrep.2020.02.099.

ACKNOWLEDGMENTS

We are grateful to the members of the Centre for Gnotobiology of the Institut Pasteur for technical support with the mice with a modified/controlled microbiota. We thank all of the Lledo lab members, Prof. Chantal Henry and Dr. Maud Pascal in particular, and Dr. Nicolas Kuperwasser for helpful comments. This work was funded by the Investissements d'Avenir program (grants ANR-11-IDEX-0004-02 and ANR-10-LABX-73), the Agence Nationale de la Recherche (grant ANR-15-CE37-0004-01), AG2R La Mondiale, and Mutuelle de la Région Lyonnaise. We also thank the Fondation des Gueules Cassées, École des Neurosciences de Paris, and Labex Revive for fellowships (to E.S. and S.S.).

AUTHOR CONTRIBUTIONS

Conceptualization, E.S.; Methodology, E.S., G.C., and L.K.; Investigation, E.S., G.C., L.K., M.B., and C.M.; Software, S.S.; Writing – Original Draft, E.S.; Writing – Review & Editing, E.S. and P.-M.L.; Funding Acquisition, P.-M.L., G.E., and E.S.; Resources, P.-M.L. and G.E.; Supervision, E.S. and P.-M.L.

DECLARATION OF INTERESTS

The authors declare no competing interests.

Received: May 17, 2019
Revised: November 25, 2019
Accepted: February 26, 2020
Published: March 17, 2020

REFERENCES

Agus, A., Planchais, J., and Sokol, H. (2018). Gut microbiota regulation of tryptophan metabolism in health and disease. Cell Host Microbe *23*, 716–724.

Anacker, C., Luna, V.M., Stevens, G.S., Millette, A., Shores, R., Jimenez, J.C., Chen, B., and Hen, R. (2018). Hippocampal neurogenesis confers stress resilience by inhibiting the ventral dentate gyrus. Nature *559*, 98–102.

Boldrini, M., Santiago, A.N., Hen, R., Dwork, A.J., Rosoklija, G.B., Tamir, H., Arango, V., and John Mann, J. (2013). Hippocampal granule neuron number and dentate gyrus volume in antidepressant-treated and untreated major depression. Neuropsychopharmacology *38*, 1068–1077.

Bouknight, R.R., and Sadoff, H.L. (1975). Tryptophan catabolism in Bacillus megaterium. J. Bacteriol. *121*, 70–76.

Campbell, S., Marriott, M., Nahmias, C., and MacQueen, G.M. (2004). Lower hippocampal volume in patients suffering from depression: a meta-analysis. Am. J. Psychiatry *161*, 598–607.

Clarke, G., Grenham, S., Scully, P., Fitzgerald, P., Moloney, R.D., Shanahan, F., Dinan, T.G., and Cryan, J.F. (2013). The microbiome-gut-brain axis during early life regulates the hippocampal serotonergic system in a sex-dependent manner. Mol. Psychiatry *18*, 666–673.

Cole, J.R., Wang, Q., Cardenas, E., Fish, J., Chai, B., Farris, R.J., Kulam-Syed-Mohideen, A.S., McGarrell, D.M., Marsh, T., Garrity, G.M., and Tiedje, J.M. (2009). The Ribosomal Database Project: improved alignments and new tools for rRNA analysis. Nucleic Acids Res. *37*, D141–D145.

De Palma, G., Blennerhassett, P., Lu, J., Deng, Y., Park, A.J., Green, W., Denou, E., Silva, M.A., Santacruz, A., Sanz, Y., et al. (2015). Microbiota and host determinants of behavioural phenotype in maternally separated mice. Nat. Commun. *6*, 7735.

Desbonnet, L., Clarke, G., Traplin, A., O'Sullivan, O., Crispie, F., Moloney, R.D., Cotter, P.D., Dinan, T.G., and Cryan, J.F. (2015). Gut microbiota depletion from early adolescence in mice: Implications for brain and behaviour. Brain Behav. Immun. *48*, 165–173.

Fernstrom, J.D., Langham, K.A., Marcelino, L.M., Irvine, Z.L., Fernstrom, M.H., and Kaye, W.H. (2013). The ingestion of different dietary proteins by humans induces large changes in the plasma tryptophan ratio, a predictor of brain tryptophan uptake and serotonin synthesis. Clin. Nutr. *32*, 1073–1076.

Gould, E. (1999). Serotonin and hippocampal neurogenesis. Neuropsychopharmacology *21* (*Suppl 2*), 46S–51S.

Ibarguen-Vargas, Y., Surget, A., Touma, C., Palme, R., and Belzung, C. (2008). Multifaceted strain-specific effects in a mouse model of depression and of antidepressant reversal. Psychoneuroendocrinology *33*, 1357–1368.

Ioannidis, J.P. (2008). Effectiveness of antidepressants: an evidence myth constructed from a thousand randomized trials? Philos. Ethics Humanit. Med. *3*, 14.

Jacobsen, J.P., Siesser, W.B., Sachs, B.D., Peterson, S., Cools, M.J., Setola, V., Folgering, J.H., Flik, G., and Caron, M.G. (2012). Deficient serotonin neurotransmission and depression-like serotonin biomarker alterations in tryptophan hydroxylase 2 (Tph2) loss-of-function mice. Mol. Psychiatry *17*, 694–704.

Jacobsen, J.P., Rudder, M.L., Roberts, W., Royer, E.L., Robinson, T.J., Oh, A., Spasojevic, I., Sachs, B.D., and Caron, M.G. (2016). SSRI augmentation by 5-hydroxytryptophan slow release: Mouse pharmacodynamic proof of concept. Neuropsychopharmacology *41*, 2324–2334.

Jiang, H., Ling, Z., Zhang, Y., Mao, H., Ma, Z., Yin, Y., Wang, W., Tang, W., Tan, Z., Shi, J., et al. (2015). Altered fecal microbiota composition in patients with major depressive disorder. Brain Behav. Immun. *48*, 186–194.

Kassebaum, N.J.; GBD 2015 DALYs and HALE Collaborators (2016). Global, regional, and national disability-adjusted life-years (DALYs) for 315 diseases and injuries and healthy life expectancy (HALE), 1990-2015: a systematic analysis for the Global Burden of Disease Study 2015. Lancet *388*, 1603–1658.

Katsimpardi, L., Gaitanou, M., Malnou, C.E., Lledo, P.M., Charneau, P., Matsas, R., and Thomaidou, D. (2008). BM88/Cend1 expression levels are critical for proliferation and differentiation of subventricular zone-derived neural precursor cells. Stem Cells *26*, 1796–1807.

Langfelder, P., and Horvath, S. (2008). WGCNA: an R package for weighted correlation network analysis. BMC Bioinformatics *9*, 559.

Marin, I.A., Goertz, J.E., Ren, T., Rich, S.S., Onengut-Gumuscu, S., Farber, E., Wu, M., Overall, C.C., Kipnis, J., and Gaultier, A. (2017). Microbiota alteration is associated with the development of stress-induced despair behavior. Sci. Rep. *7*, 43859.

Möhle, L., Mattei, D., Heimesaat, M.M., Bereswill, S., Fischer, A., Alutis, M., French, T., Hambardzumyan, D., Matzinger, P., Dunay, I.R., and Wolf, S.A. (2016). Ly6C(hi) Monocytes Provide a Link between Antibiotic-Induced Changes in Gut Microbiota and Adult Hippocampal Neurogenesis. Cell Rep. *15*, 1945–1956.

Naseribafrouei, A., Hestad, K., Avershina, E., Sekelja, M., Linløkken, A., Wilson, R., and Rudi, K. (2014). Correlation between the human fecal microbiota and depression. Neurogastroenterol. Motil. *26*, 1155–1162.

Nestler, E.J., Barrot, M., DiLeone, R.J., Eisch, A.J., Gold, S.J., and Monteggia, L.M. (2002). Neurobiology of depression. Neuron *34*, 13–25.

O'Mahony, S.M., Clarke, G., Borre, Y.E., Dinan, T.G., and Cryan, J.F. (2015). Serotonin, tryptophan metabolism and the brain-gut-microbiome axis. Behav. Brain Res. *277*, 32–48.

Perera, T.D., Coplan, J.D., Lisanby, S.H., Lipira, C.M., Arif, M., Carpio, C., Spitzer, G., Santarelli, L., Scharf, B., Hen, R., et al. (2007). Antidepressant-induced neurogenesis in the hippocampus of adult nonhuman primates. J. Neurosci. *27*, 4894–4901.

Ressler, K.J., and Nemeroff, C.B. (2000). Role of serotonergic and noradrenergic systems in the pathophysiology of depression and anxiety disorders. Depress. Anxiety *12* (*Suppl 1*), 2–19.

Sachs, B.D., Jacobsen, J.P., Thomas, T.L., Siesser, W.B., Roberts, W.L., and Caron, M.G. (2013). The effects of congenital brain serotonin deficiency on responses to chronic fluoxetine. Transl. Psychiatry *3*, e291.

Sahay, A., and Hen, R. (2007). Adult hippocampal neurogenesis in depression. Nat. Neurosci. *10*, 1110–1115.

Santarelli, L., Saxe, M., Gross, C., Surget, A., Battaglia, F., Dulawa, S., Weisstaub, N., Lee, J., Duman, R., Arancio, O., et al. (2003). Requirement of hippocampal neurogenesis for the behavioral effects of antidepressants. Science *301*, 805–809.

Schmuckermair, C., Gaburro, S., Sah, A., Landgraf, R., Sartori, S.B., and Singewald, N. (2013). Behavioral and neurobiological effects of deep brain stimulation in a mouse model of high anxiety- and depression-like behavior. Neuropsychopharmacology *38*, 1234–1244.

Siesser, W.B., Sachs, B.D., Ramsey, A.J., Sotnikova, T.D., Beaulieu, J.M., Zhang, X., Caron, M.G., and Gainetdinov, R.R. (2013). Chronic SSRI treatment exacerbates serotonin deficiency in humanized Tph2 mutant mice. ACS Chem. Neurosci. *4*, 84–88.

Surget, A., Saxe, M., Leman, S., Ibarguen-Vargas, Y., Chalon, S., Griebel, G., Hen, R., and Belzung, C. (2008). Drug-dependent requirement of hippocampal neurogenesis in a model of depression and of antidepressant reversal. Biol. Psychiatry *64*, 293–301.

Surget, A., Tanti, A., Leonardo, E.D., Laugeray, A., Rainer, Q., Touma, C., Palme, R., Griebel, G., Ibarguen-Vargas, Y., Hen, R., and Belzung, C. (2011). Antidepressants recruit new neurons to improve stress response regulation. Mol. Psychiatry *16*, 1177–1188.

Velagapudi, V.R., Hezaveh, R., Reigstad, C.S., Gopalacharyulu, P., Yetukuri, L., Islam, S., Felin, J., Perkins, R., Borén, J., Oresic, M., and Bäckhed, F. (2010). The gut microbiota modulates host energy and lipid metabolism in mice. J. Lipid Res. *51*, 1101–1112.

Zhang, L.S., and Davies, S.S. (2016). Microbial metabolism of dietary components to bioactive metabolites: opportunities for new therapeutic interventions. Genome Med. *8*, 46.

Zheng, P., Zeng, B., Zhou, C., Liu, M., Fang, Z., Xu, X., Zeng, L., Chen, J., Fan, S., Du, X., et al. (2016). Gut microbiome remodeling induces depressive-like behaviors through a pathway mediated by the host's metabolism. Mol. Psychiatry *21*, 786–796.

STAR★METHODS

KEY RESOURCES TABLE

REAGENT or RESOURCE	SOURCE	IDENTIFIER
Antibodies		
Rabbit polyclonal anti-DCX	Abcam	Cat#ab18723; RRID: AB-732011
Chicken polyclonal anti-DCX	Abcam	Cat# Ab153668; RRID: AB_2728759
Rabbit polyclonal anti-Ki67	Abcam	Cat# ab15580; RRID: AB_443209
Rabbit polyclonal anti-IDO	Abcam	Cat# ab106134; RRID: AB_10860804
Rabbit polyclonal anti-TPH	Abcam	Cat# ab30574; RRID: AB_778658
Goat polyclonal anti-SERT	Abcam	Cat# ab130130; RRID: AB_11157503
Rabbit monoclonal anti-MAOA	Abcam	Cat# ab126751; RRID: AB_11129867
Mouse monoclonal anti-DDC	Abcam	Cat# ab49916; RRID: AB_2088940
Goat polyclonal anti-IL1beta/IL-1F2	R and D systems	Cat# AF-401-NA; RRID: AB_416684
Rabbit polyclonal anti-Iba1	Wako	Cat# 019-19741; RRID: AB_839504
Rabbit anti-Mouse secondary Alexa Fluor 488	Thermo Fischer scientific	Cat# A-11041; RRID: AB_2534098
Goat anti-Chicken secondary Alexa Fluor 568	Thermo Fischer scientific	Cat# A-11041; RRID: AB_2534098
Goat anti-rabbit IgG (H + L)-HRP conjugate antibody	Bio-Rad	Cat# 1706515; RRID: AB_2617112
Rabbit anti-goat IgG (H+L)-HRP	Thermo Fischer scientific	Cat# 81-1620; RRID: AB_2534006
Goat anti-mouse IgG1 – heavy chain (HRP)	Abcam	Cat# ab97240; RRID: AB_10695944
Chemicals, Peptides and Recombinant Proteins		
Vancomycin	Merck	Cat#V2002; CAS Number: 1404-93-9
Ampicillin	Merck	Cat#A9518; CAS Number: 69-52-3
Colistin	Merck	Cat#C4461; CAS Number: 1264-72-8
Amphotericin B	Merck	Cat#A9528; CAS Number: 1397-89-3
Fluoxetine hydrochloride	Anawa	Cat#A2436; Cat# BG0197
5-hydroxy tryptophan	Merck	Cat#H9772; CAS Number: 4350-09-8
Normal goat serum	Sigma-Aldrich	Cat#G9023; CAS Number: N/A
Fluoromount aqueous mounting medium	Sigma-Aldrich	Cat#F4680; CAS Number: N/A
4′,6′-diamidino-2-phenylindole (DAPI)	Sigma-Aldrich	Cat#10236276001; CAS Number: 0028718903
Pierce BCA Protein Assay Kit	Thermo Fischer Scientific	Cat#23227; CAS Number: 7758-99-8
NuPAGE LDS Sample Buffer (4X)	Thermo Fischer Scientific	Cat#NP0007; CAS Number: N/A
NuPAGE 4-12% Bis-Tris Protein Gels, 1.0 mm, 17-well	Thermo Fischer Scientific	Cat#NP0329PK2; CAS Number: N/A
NuPAGE 4-12% Bis-Tris Protein Gels, 1.0 mm, 10-well	Thermo Fischer Scientific	Cat# NP0321BOX; CAS Number: N/A
Trans-Blot Turbo RTA Mini PVDF Transfer Kit	Biorad	Cat #1704272; CAS Number: N/A
Immobilon Crescendo Western HRP Substrate	Millipore	Cat #WBLUR0100; CAS Number: N/A
RIPA lysis and extraction buffer	Thermo Fischer Scientific	Cat#89901; CAS Number: N/A
cOmplete Protease Inhibitor Cocktail	Roche	Cat#11697498001; CAS Number: N/A
cOmplete ULTRA Tablets, Mini, EASYpack Protease Inhibitor Cocktail	Roche	Cat#5892970001; CAS Number: N/A
Triton X-100 solution	Sigma-Aldrich	Cat# 9002-93-1; CAS Number 9002-93-1
Critical Commercial Assays		
Mouse TNF-alpha platinum ELISA 2 × 96 tests Kit	Thermo Fisher Scientific	Cat# BMS607/3TWO; RRID: AB_2575664
Mouse IL-6 platinum ELISA 2 × 96 tests Kit	Thermo Fisher Scientific	Cat# BMS603/2TWO; RRID: AB_2575650
FastDNA Spin kit	MP Biomedicals	Cat#MP116540600; RRID: N/A
Software and Algorithms		
Fiji	ImageJ	https://imagej.nih.gov/ij

(*Continued on next page*)

Continued

REAGENT or RESOURCE	SOURCE	IDENTIFIER
Icy open source software	Icy	http://icy.bioimageanalysis.org
R software FactoMineR package	R Core Team 2017	https://cran.r-project.org/web/packages/FactoMineR/index.html
R software gplots package	R Core Team 2017	https://cran.r-project.org/web/packages/gplots/index.html
MATLAB	Mathworks Inc. 2015 release	RRID: SCR_001622
ZEN Digital Imaging for Light Microscopy	Zeiss	RRID: SCR_013672
Graphpad	Prism version 6	RRID: SCR_002798
EthoVision XT	Noldus	RRID: SCR_000441
Codes and scripts in R and MATLAB		Codes available upon request: https://github.com/SohamSahaNeuroscience/Microbiota-analysis

LEAD CONTACT AND MATERIALS AVAILABILITY

Further information and requests for resources and reagents should be directed to and will be fulfilled by the Lead Contact, Eleni Siopi (eleni.siopi@inserm.fr). This study did not generate new unique reagents.

EXPERIMENTAL MODEL AND SUBJECT DETAILS

Animals

Experiments were performed using adult (8 week old) male C57BL/6J mice purchased from Janvier labs (St Berthevin, France). They were housed in groups of five and maintained in controlled room temperature (22-24°C) and humidity, 12h/12h light /dark cycle, with lights on at 7:00 AM, *ad libitum* access to dry food pellets and water, at the Pasteur Institute animal care facility, officially registered for experimental studies on rodents. All animal experiments were designed according to the 3R's rules and approved by the local ethical committee on animal experimentation of the Institut Pasteur (project CETEA #2013-0062 and #2016-0023) and supervised by the French Ministry of Research.

Unpredictable chronic mild stress (UCMS) procedure

Mice were chronically exposed to interchanging unpredictable mild stressors, administered daily in random order for 8 weeks, using a modified version of a previous protocol (Ibarguen-Vargas et al., 2008). Two stressors were applied daily, one in the morning and one in the evening, and none of the stressors involved food or water deprivation. The different stressors are listed below: (1) cage shaking (1 time, 5 min), (2) cage tilting 45°C (2 h), (3) moist bedding (2 h), (4) overnight illumination (12 h), (5) reversing day and night (24 h), (6) restraint (30min), (7) recurrent cage change (2 h), (8) predator odor (rat urine). Behavioral experiments were performed over a period of 1 week while the animals were still undergoing UCMS, starting at week 8 of the UCMS protocol. At week 9, mice were euthanized and randomly allocated to histological or molecular endpoints using a counter-balanced design. The control animals were socially housed (5 animals/cage) and left undisturbed unless necessary procedures including routine cleaning.

Treatments

Microbiota recipient mice (8 weeks of age) were treated with an antibiotic (abx) cocktail, consisting of a mixture of ampicillin (1mg/ml), streptomycin (5mg/ml), colistin (1mg/ml), vancomycin (0.5mg/ml) and amphotericin (0.1 mg/ml). The abx treatment lasted one week and ceased 24h prior to microbiota inoculation. Fresh fecal samples (1 mg in 5 mL sterile PBS) were used for the transfer protocol, harvested from either control (CT) or UCMS mice. Recipient mice received the fecal suspension (300 μL per mouse) by oral gavage at 1 and 4 days following abx discontinuation, and were maintained in isolators from one day prior abx discontinuation and up to the onset of behavioral testing. FLX (18 mg/kg/day) and 5-hydroxytryptophan (5-HTP, 100 mg/kg/day) were administered in the drinking water for 4 weeks as previously described (Siesser et al., 2013; Jacobsen et al., 2016).

Experimental sets

A total of 150 mice were used in this study, allocated in four separate experimental sets, as described below:

Experimental set 1

Analysis of GM populations, behavior, neurogenesis and metabolic changes following microbiota transfer from UCMS mice to abx-treated mice. Four groups of mice (n = 10/group) were included in this set: a control (CT) group, a group of mice that sustained an 8-week chronic stress protocol (UCMS group), and two groups of abx-treated mice that were inoculated with fecal microbiota

from either CT mice (CT-tr) or UCMS mice (UCMS-tr). All subjects were subjected to behavioral testing. Six mice per group were randomly assigned for neurogenesis analysis and five mice per group for the GM and serum metabolite analysis.

Experimental set 2

Study of the effect of FLX on anxiety and depression-like behavior, HpC neurogenesis and Trp metabolites in microbiota donor mice. Three groups of mice were included in this set: a control group (CT) (n = 10), and two groups of mice that sustained an 8-week UCMS protocol and that were treated or not with FLX [UCMS+FLX (n = 12) and UCMS (n = 10) groups respectively]. All subjects were subjected to behavioral testing. Six-seven mice per group were randomly assigned for neurogenesis analysis and five mice per group for molecular and metabolite analysis.

Experimental set 3

Study of the effect of 5-HTP on behavior, HpC neurogenesis, Trp metabolism (brain, gut, serum) and FLX efficacy, following UCMS-microbiota inoculation. Five groups of microbiota recipient mice were included in this set: a CT-tr (n = 13), a UCMS-tr (n = 15) and a UCMS-tr+FLX (n = 10) group, as described in experimental set 1 above, and two groups of UCMS-tr mice that received either 5-HTP alone (UCMS-tr+5-HTP group, n = 10) or adjunct to FLX (UCMS-tr+5-HTP+FLX group, n = 10). All the subjects were subjected to behavioral testing. Six-eight subjects were randomly assigned for neurogenesis analysis and five mice per group for molecular and metabolic analysis.

Experimental set 4

Study of the effect of abx on GM composition, anxiety and depression-like behavior, neurogenesis, Trp metabolism (serum and gut) and neural stem cell differentiation. A total of 10 mice/group were used in this study. Ten mice per group were used for the behavioral assessment and five mice per group were randomly assigned for molecular and metabolite analysis.

METHOD DETAILS

Behavioral testing

For all behavioral tests, mice were transferred to the testing room at least 1 h before testing. Animals were tested in random order during each testing period and equipment was thoroughly cleaned with 80% ethanol between trials to minimize scents. Microbiota donor mice were tested over a period of 1 week while the animals sustained the last week of UCMS (Figure 1B). Microbiota recipient mice were tested upon exit from the isolators (Figure 1C). All analyses were performed with the experimenter blind to the experimental condition.

Tail suspension test

Mice were suspended at approximately one-third from the end of the tail, using regular tape, to an aluminum bar connected to a strain gauge. The mouse was suspended from a 30 cm high metal rod. The test was recorded during a 5 minute period. Upon viewing of the video recordings, the total time spent in an immobile posture was measured. Mice were considered immobile when they stopped struggling to escape and hung passively, motionless, by the tail. Longer periods of immobility are associated with depressive states.

Forced swim test

Mice were placed into a clear Plexiglas cylinder (25 cm in height and 10 cm in diameter) filled up to two thirds with water (24°C), for a 5-minute session. The sessions were video-recorded and the duration of immobility was measured upon viewing of the video recordings. Immobility was defined as the lack of active movements except from those required for floating.

Open field

Animals were placed in white Plexiglas containers (43 × 43 cm^2) and behaviors were recorded by a video camera during 30 min. A tracking system (Noldus Ethovision XT 3.0) was used to map center and periphery zones and to calculate the time spent in each zone. The time spent in the center and the total distance traveled were calculated as measures of anxiety behavior and ambulatory activity respectively.

Elevated plus maze

The test was conducted using a plus-cross-shaped apparatus made of black Plexiglas, which was elevated 58 cm above the floor and comprised two open and two closed arms (30 × 6 cm) that extended from a central platform (7 × 7 cm). The Noldus Ethovision 3.0 tracking system was used to record behavior for 5 min. The number of entries and the total time spent in the open arms of the apparatus were calculated as measures of anxiety.

Light and dark box

A two-compartment box containing a dark chamber (black walls with upper lid) and a light chamber (~300 lux, white Plexiglas walls, no upper lid) was used. The chambers were connected by a 10 × 10 cm door in the middle of the wall. Animals were placed in one corner of the light chamber facing the wall and were allowed to freely explore for 10 min. The Noldus Ethovision 3.0 tracking system was used to record behavior. The number of entries and time spent in the light chamber were estimated as measures of anxiety.

Animal sacrifice and tissue collection

Mice allocated to immunofluorescence studies were deeply anesthetized with a mixture of xylazine-ketamine (10mg/g bw, Sanofi, Bagneux, France) and were perfused transcardially with a solution containing 0.9% NaCl at 37°C, followed by 4% paraformaldehyde (PFA) in phosphate buffer (pH 7.3). All animals were sacrificed between the hours of 10am and 12 noon. Animals were sacrificed in randomized order to minimize experimental bias. The mice were then decapitated, and the brain was carefully removed. Mice allocated to molecular biology analysis, were deeply anesthetized with xylazine-ketamine (10mg/g bw). Approximately 1 mL of blood was taken via cardiac puncture. The whole HpC was carefully dissected, immediately snap-frozen in liquid-nitrogen, and maintained at 80°C until further processing. The blood was put into an ice-cold tube and placed directly into wet ice before centrifugation at 14,000 rpm for 10 minutes for serum collection. The serum was used for metabolic measurements and for the neurosphere assays. Small intestines were collected upon sacrifice and the stool was pushed out. The samples were immediately snap-frozen in liquid nitrogen and moved to 80°C until further processing. Fecal samples were harvested at the end of the UCMS protocol in donor mice and upon exit from the isolators in recipient mice.

Neural stem cell cultures

Neurosphere cultures were prepared from the subventricular zone area of postnatal day 5 C57/BL6J mice, as previously described (Katsimpardi et al., 2008). After 7 days in culture, floating neurospheres were trypsin-dissociated and allowed to reform spheres at least three times before further use. Neural stem cell cultures (neurospheres) were maintained in DMEM/F12 medium with EGF and basic FGF (both at 20ng/ml final concentration). For the differentiation assay, neurospheres were plated on poly-lysine/laminin coated coverslips in serum-free, growth-factor-free DMEM/F12 medium to initiate adhesion. To assess the effects of different serum conditions on differentiated neurospheres, 4 μL of sera derived from CT, UCMS, CT-tr and UCMS-tr mice were added to 500 μL of culture medium for 4 days. At the end of the experiment, neurospheres were fixed with 4% paraformaldehyde for 30 minutes. For each condition 4 different culture wells were used. All incubations took place in 24-well plates.

Western blots

Neurospheres, brains and gut tissue were lysed in RIPA lysis buffer (25mM Tris-HCl pH 7.6, 150 mM NaCl, 1% NP-40, 1% sodium deoxycholate, 0.1% SDS; Pierce Thermo Scientific) supplemented with protease (cOmplete, Sigma) and phosphatase (phosSTOP, Sigma) inhibitors. Protein concentration was measured with Pierce BCA protein Assay Kit (ThermoFischer Scientific) prior to the western blot assay. Tissue lysates were mixed with 4x NuPage LDS loading buffer (Invitrogen) and reducing agent (Invitrogen NP0004), and proteins were separated on a 4%–12% SDS-polyacrylamide gradient gel (Invitrogen NP0329) and subsequently transferred by semi-dry or liquid transfer onto a PVDF membrane (Trans-blot Turbo Mini PVDF, Biorad). The blots were blocked in 3% BSA in Tris-buffered saline with Tween (TBS-T) and incubated with mouse anti-actin (1:6000, A5441, Sigma). To detect protein signal, the following Horseradish peroxidase–conjugated secondary antibodies were used: Goat Anti-Rabbit IgG (H+L)-HRP Conjugate (1:6000, #1706515, Biorad) and Goat Anti-Mouse IgG1 heavy chain (HRP) (1:6000, ab97240, abcam) and rabbit anti-goat IgG (H+L)-HRP (1:6000, # 31402 Invitrogen). Chemiluminescence detection of proteins was performed with Crescendo Western HRP Substrate (Merck Millipore) with a Chemidoc Imaging System (Biorad). Bands were quantified using the Fiji (ImageJ) software.

Sandwich ELISA immunoassays

The following kits were used for ELISA immunoassays: mouse IL-6 (BMS603/2, Invitrogen), and mouse TNF-α (BMS607/3, Invitrogen). All immunoassays were performed and analyzed according to the manufacturer's instructions. Data were normalized based on protein concentrations, measured by a BCA assay.

Immunofluorescence

Perfused brains were cut at 40-micron thick coronal sections using a vibrating microtome (VT1000S, Leica). Immunostaining was performed on free-floating sections. Non-specific staining was blocked by 0.2% Triton and 10% goat serum albumin (Sigma-Aldrich). Sections were incubated with the following primary antibodies at 4°C: rabbit anti-DCX (1:400, Abcam ab18723), chicken anti-DCX (1:400, Abcam ab1536668) and rabbit anti-Ki67 (1:200, Abcam ab15580). For neurosphere cultures, cells were fixed on coated coverslips. They were pre-incubated in 10% normal goat serum, 0.1% Triton X-100 in PBS for 1h and were then incubated overnight at 4°C with chicken polyclonal anti-DCX (1:400, Abcam ab153668). Sections or cells were then incubated with secondary antibodies (biotinylated or Alexa-conjugated secondary antibodies at 1:1000, Jackson ImmunoResearch Laboratories) at room temperature. Fluorescent sections or cells were stained with the nuclear dye 4′,6′-diamidino-2-phenylindole (DAPI) and then mounted using Fluoromount aqueous mounting medium (Sigma-Aldrich).

Confocal imaging and quantification

Images were acquired using a confocal laser-scanning microscope (LSM 710, Zeiss, France) with Zen Imaging software (Zeiss). Z stacks of the dentate gyrus were obtained (step size: 1 μm) using sequential tile scanning. Cell counting was performed using the Icy open source platform (http://icy.bioimageanalysis.org). Values are expressed as the mean number of $Ki67^+$ or DCX^+ cell counts in 8-10 sections per animal.

Microbial DNA extraction and 16S sequencing

Fecal samples were collected in autoclaved Eppendorf tubes and were stored at 80°C until further processing. DNA was extracted using the FastDNA Spin kit (MP Biomedicals) according to the manufacturer's instructions. DNA concentrations were determined using a Nanodrop (Thermo Scientific). Microbial profiling was assessed by 16S rRNA metagenomic analysis, performed on an Illumina MiSeq instrument using the v3 reagent kit. PCR amplificons targeted the V3-V4 region of the 16 s rDNA (Biomics platform, Institut Pasteur). Following purification, a second PCR amplification was performed to barcode samples with Nextera XT Index Primers. Libraries were loaded onto a MiSeq instrument and sequencing was performed. De-multiplexing of the sequencing samples was performed on the MiSeq and individual FASTQ files were recovered for analysis.

16S sequencing data analysis

Sequences were clustered into operational taxonomic units (OTU) and annotated with the MASQUE pipeline (https://github.com/aghozlane/masque) as previously described (Cole et al., 2009). The final list of 16S rRNA targeted amplicons were converted into the negative logarithm of the expressions of the bacterial taxa (phylum and family). Final data were expressed as the average (represented in a heatmap) and sum (represented in barplots) of the negative logarithm of OTU expression across experimental conditions. All data indexing, segregation and heatmap plotting were performed using custom-made scripts in MATLAB (Mathworks Inc., 2015 release). Further statistical tests were conducted in Prism software (GraphPad). The microbiota profiles obtained were further characterized using the following methods:

a. Principal coordinate analysis (PCoA): We used the Bray-Curtis metric to calculate the sample distance across the four conditions: CT, CT-tr, UCMS and UCMS-tr. The Bray-Curtis metric is given as: Bcij = 1-(2Cij/(Si+Sj)), where Cij is the sum of the minimal relative abundance for only those species in common between experimental protocols; Si and Sj being the total number of OTUs counted at these conditions. The Bray-Curtis distance has a bound value between 0 and 1. PcoA plots with PC1 and PC2 are shown in a scatter-plot to cluster samples with lesser distance metric.
b. Weighted Gene Correlation Network Analysis (WGCNA). In order to gain insight into specific behaviors of bacterial composition in different experimental protocols, we performed WCGNA applied to microbial communities, by adapting the methods described in Langfelder and Horvath (2008). Briefly, WCGNA identifies clusters of variables (relative abundance of OTUs) which are correlated to given traits (bacterial phyla or families) using hierarchical clustering approach, weighted adjacency functions, topological overlap measures, and a dynamic tree cutting method. The following parameters were used:

Variables	Values
Minimum module size (minMod)	10
Power of scale free network (ds)	3
Dynamic Cut Height	0.99999
Soft threshold	0.15

Each OTU relative expression was represented by a node in a vast network and their adjacency (a score between 0 and 1). A weighted Pearson's correlation was used as a measurement of co-expression for each bacterial family. This takes into account the actual strength of the connection so that an adjacency matrix could be constructed. The adjacency matrix was determined using a 'soft threshold', which is given by: Adjacency = 0.5 x (1+ r)sft, where r is the Pearson's correlation and sft is the soft threshold as shown in the table above. A scale-free topology model is generated by raising the co-expression similarity to a power: aij = sijß with $\beta \geq 1$. Aij is a weighted adjacency between two genes is proportional to their similarity on a logarithmic scale, log (aij) = $\beta \times$ log (sij). PickSoftThreshold package in R was used (our data had $\beta = 3$). The adjacency matrix is then used to generate a Topological Overlap Measure (TOM), describing the relative co-occurrence between two nodes and placing it in the framework of the entire network. The whole network connectivity distribution is shown as a network heatmap, and the branches in the hierarchical clustering dendrograms correspond to modules. The modules were color-coded and data was segregated from each module to classify them into major bacterial families.

c. Autocorrelation among modules: The significant modules (or clusters) were determined using an ANOVA test on the cluster z-scores across the experimental conditions: CT, CT-tr, UCMS and UCMS-tr. We identified 5 modules, cluster 2, 3, 4, 9 and 10, based on the criteria above. In order to account for the degree of similarity between the components in the modules and cross-sectional similarities in the observed data, an autocorrelation of the obtained clusters was performed and shown as a correlation matrix. The mean z-scores of the significant clusters across the experiments were also calculated. The common phyla within all the clusters were the most prominent Firmicutes and Bacteroidetes, although less abundant families like Proteobacteria, Actinobacteria and Tenericutes were also common.

d. Correlation of GM with metabolites. Metabolites related to Trp metabolism were correlated to the cluster z-scores of each Phylum/family in each condition to check for coincidental variability of bacterial relative expression and metabolite profiling. Pearson's r was used to generate the correlation matrix across conditions and the identified clusters. We isolated the Firmicutes and Bacteroidetes in each cluster and correlated them to Trp expression profile for the experimental conditions: CT, UCMS, CT-tr and UCMS-tr.

Serum extraction and metabolite analysis

Blood samples were collected (Microvette 200 Z-Gel, Fischer scientific) and centrifuged at 14,000 rpm for 10 minutes at 4°C. The clot was removed and serum was transferred into a clean polypropylene tube using a Pasteur pipette. Serum samples were then stored at −80°C. Two series of serum samples were analyzed in two different GC/MS, LC/MS and LC/MS/MS platforms (Metabolon Inc, California, USA and metabolic platform at SFR Necker, France). Hippocampus and gut samples were analyzed at the metabolic platform at SFR Necker, France. Protein fractions were removed by serial extractions with organic aqueous solvents, concentrated using a TurboVap system (Zymark) and vacuum dried. For LC/MS and LC/MS/MS, samples were reconstituted in acidic or basic LC-compatible solvents containing > 11 injection standards and run on a Waters ACQUITY UPLC and Thermo-Finnigan LTQ mass spectrometer, with a linear ion-trap front-end and a Fourier transform ion cyclotron resonance mass spectrometer back-end. For GC/MS, samples were derivatized under dried nitrogen using bistrimethyl-silyl-trifluoroacetamide and analyzed on a Thermo-Finnigan Trace DSQ fast-scanning single-quadrupole mass spectrometer using electron impact ionization. Chemical entities were identified by comparison to metabolomic library entries of purified standards. Data were analyzed following log transformation and NA values were replaced with minimum observed values when necessary. Principal component analysis (PCA) was applied on the 710 assessed metabolites. The six first principal components (PC) explained 63.78% of the variance of the data, and PC1 and PC2 accounted for 19.6% and 17.63% of the variance respectively. To get an insight of the metabolic pathways represented within each PC, we looked at the correlation coefficients between the PC and the metabolites. We kept the metabolites that were correlated to a PC with a coefficient superior to 0.65. PCA and heatmap plotting was performed using the R software (R Core Team 2017, FactoMineR and gplots packages).

QUANTIFICATION AND STATISTICAL ANALYSIS

Data were analyzed with GraphPad Prism (version 6, San Diego, USA), with $p < 0.05$ considered statistically significant. Statistical parameters and the exact number of animals employed in each study are reported in the Experimental sets part of the Experimental Models and Subject details. Statistical significance is reported in the figure legends. All data were expressed as mean ± SEM. Data were analyzed using the non-parametric Mann-Whitney test or one-way analysis of variance (ANOVA) followed by Bonferonni post hoc test when appropriate. Linear regression was used to determine relationships between variables and a Pearson's correlation was used to calculate statistically significant relationships.

DATA AND CODE AVAILABILITY

The codes generated during this study are available upon request at https://github.com/SohamSahaNeuroscience/Microbiota-analysis.